國立成功大學

太空與電漿科學研究所

112 年年度報告

National Cheng Kung University

Department of Photonics

專題生：劉倢伶

指導教授：張博宇 博士

日期：2024/02-2024/08

Abstract

This report summarizes the work conducted over six months, focusing on the development of a 3-axis B-dot probe for magnetic field measurement in the Formosa Integrated Research Spherical Tokamak (FIRST). The study emphasizes designing, constructing, and calibrating the probe, essential for measuring dynamic magnetic fields in magnetic confinement fusion experiments. The probe consists of three orthogonal loops, each with 32 turns of enameled wire around a 10×10×10 mm^3 core, enabling simultaneous measurement of three magnetic field components. To calibrate the probe, a solenoid was employed to generate a known magnetic field, driven by a high-pulse current from a charged capacitor. The induced voltage in the probe loops was measured and correlated with the solenoid's magnetic field, resulting in calibration factors aligning with theoretical expectations. Noise analysis showed minimal interference, and the calibration process confirmed the inverse relationship between the probe's area and sensitivity. The report details key findings, including a calibration factor of approximately 130 and low common noise between signals, ensuring robust measurements where calibration factor $C_{calib} \equiv (NA)^{-1}$, N is the number of turn and A is the area of the loop. Future directions include the development of 3-axis Helmholtz coils for generating uniform magnetic field in any directions and modular probe arrays for flexible measurements. This work advances diagnostic tools for plasma control and physics analysis in fusion research.

Key word：magnetic field measurement

Table of contents

Chapter 1 Motivation

Accurate magnetic field measurements are crucial for diagnosing plasma behavior and ensuring effective control in magnetic confinement fusion devices. Understanding plasma dynamics in experimental operations requires precise determination of all three magnetic field components (B_x, B_y, and B_z in cartesian coordinate or fields in toroidal direction B_T, poloidal direction B_P, and vertical direction B_Z in a Tokamak). To meet these demands, we propose the development of a 3-axis B-dot probe for the Formosa Integrated Research Spherical Tokamak (FIRST). This probe, incorporating orthogonal coil designs and optimized calibration techniques, aims to deliver reliable and precise magnetic measurements under challenging experimental conditions, advancing the study of plasma confinement and control.

Chapter 2 Theories

This section introduces Faraday's Law, which explains how a changing magnetic flux induces a voltage in a loop, with the direction opposing the change (Lenz's Law). In multi-turn coils like B-dot probes, the induced voltage scales with the number of turns and is proportional to the rate of magnetic field change. By integrating this voltage and applying a calibration factor, the magnetic field can be reconstructed. A solenoid, which generates a stable and uniform magnetic field, is used as a reference for calibration, enabling accurate determination of the calibration factor by comparing measured and expected values.

2.1 Faraday's law of electromagnetic induction

Faraday's Law is a fundamental principle of electromagnetism that describes the induction of electromotive force (EMF) in a closed loop due to a time-varying magnetic flux. This principle can be mathematically expressed as:

$$V_{\text{ind}} = -\frac{d\Phi_{\text{B}}}{dt} \ . \tag{1}$$

where V_{ind} is the induced voltage (EMF), Φ_{B} represents the magnetic flux through the coil. The magnetic flux as the surface integral of the magnetic field *B* over the area *A* that it penetrates:

$$\Phi_B = \int \vec{B} \cdot d\vec{A} \ . \tag{2}$$

In the case of a multi-turn coil with *N* loops, the total induced voltage becomes:

$$V_{\text{ind}} = -N\frac{d\Phi_{\text{B}}}{dt} = -N\frac{\int \vec{B}\cdot d\vec{A}}{dt} = -NA\frac{dB}{dt} \ . \tag{3}$$

The negative sign in Faraday's Law indicates Lenz's Law, which states that the induced EMF tries to generate a current whose magnetic field opposes the change in the original magnetic flux. This principle is fundamental in applications such as electric generators, transformers, and magnetic probes like the B-dot probe.

In the case of a B-dot probe, the induced voltage is directly proportional to the rate of change of the magnetic flux. Given that the cross-sectional area remains constant, the average sampled magnetic field can be obtained as:

$$B = \frac{-1}{NA} \int V_{\text{ind}}\, dt = -C_{\text{calib}} \int V_{\text{ind}}\, dt. \tag{4}$$

where C_{calib} is the calibration factor. The calibration factor C_{calib} may deviate from $1/NA$ due to systematic errors in the area measurement. By determining C_{calib} through calibration, we can accurately reconstruct the magnetic field from the measured induced voltage.

2.2 Solenoid magnetic field equation

A solenoid can provide a uniform a uniform magnetic field and can be used as the calibration platform. For the solenoid magnetic field formula, the magnetic field *B* within a solenoid is determined by its geometric and current parameters. The relationship is expressed as:

$$B = \mu_0 \frac{N}{L} I(t). \tag{5}$$

where *B* is the magnetic field strength inside the solenoid, $\mu_0 = 4\pi \times 10^{-7}$ T·m/A is the permeability of free space, *N* is the number of turns in the solenoid, *L* is the solenoid's length, and *I*(*t*) is the current flowing through the solenoid. This equation assumes a long and tightly wound solenoid where the magnetic field is uniform along its central axis. The quantity N/L, defines the turn density of the solenoid. Together with the current *I*, the strength of the generated magnetic field is calculated. This principle plays a crucial role in the calibration of magnetic probes because the solenoid produces a controlled and measurable reference magnetic field.

By combining Faraday's Law and the solenoid magnetic field formula, the induced voltage in the probe can be directly compared to the solenoid's magnetic field. As a result, the calibration factor can be accurately obtained.

Chapter 3 Probe fabrication and experimental setup

This chapter outlines the design, fabrication, and calibration procedures of a custom-built three-axis B-dot probe used for transient magnetic field measurements. The probe structure was fabricated using 3D printing and incorporated two coil winding configurations to assess noise performance. A solenoid-based calibration system was developed to generate a controlled magnetic field, enabling accurate calibration of the probe. The experimental setup included high-current pulse generation and synchronized data acquisition using a current monitor and oscilloscope to determine the probe's calibration factor.

3.1 Three-axis B-dot probe

The fabrication process of the three-axis B-dot probe was meticulously designed to ensure both precision and reliability. The structural framework of the probe was produced using a 3D printer, yielding a compact cubic design with dimensions of 15 mm × 15 mm × 15 mm. At the center of the framework lies the main coil assembly, a smaller cube with dimensions of 10 mm × 10 mm × 10 mm, as shown in Figure. 3-1(a). Enamel-coated copper wires were selected as the coil material due to their excellent electrical and thermal properties, as shown in Figure. 3-1(b), which illustrates the actual fabricated three-axis B-dot probe.

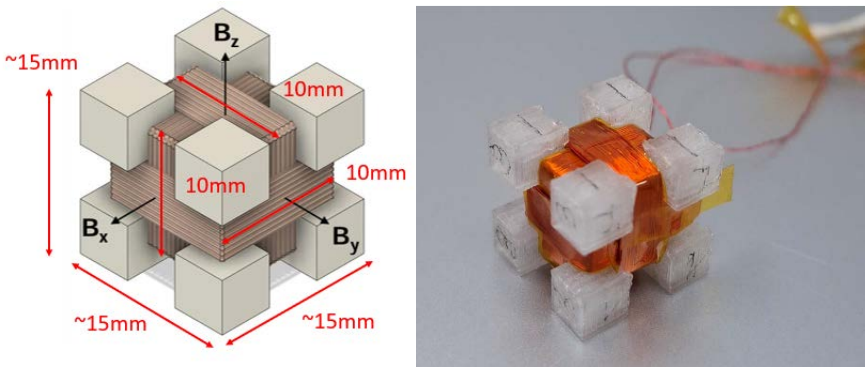

Figure. 3-1 (a) Schematic of the three-axis B-dot probe. (b) Fabricated three-axis B-dot probe.

Two distinct coil winding configurations were employed for comparison. The first configuration involves winding two coils in opposite directions along the same axis. This method aims to minimize noise interference by leveraging mutual cancellation of induced signals, as shown in Figure. 3-2.

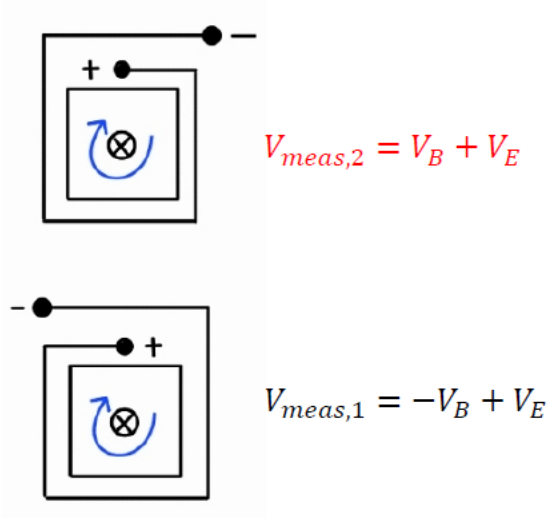

Figure. 3-2 Schematic of opposite coil winding configuration showing voltage components induced.

The second configuration features coils wound in the same direction along the same axis. After completing the winding process, the excess wire ends were twisted to ensure structural stability and reduce noise coupling. Heat-shrink tubing was used to protect the wires and secure the assembly. Finally, the wire ends were soldered to the male connector terminals to establish a robust electrical connection.

3.2 Solenoid calibration

To ensure the accuracy and reliability of the B-dot probe, a solenoid was employed to generate a stable and well-characterized magnetic field for calibration. The solenoid was constructed using a PVC tube with an outer diameter of 34 mm and an electrical wire with a cross-sectional area of 1.25 mm^2. The solenoid measured 21 cm in length and consisted of 65 turns, yielding a turn density of 309.5 turns/m.

According to Equation (5), the magnetic field inside the solenoid can be expressed as:

$$B = 3.889 \times 10^{-4} \times I(t)\ [\mathrm{T}]\ . \tag{6}$$

It shows that the magnetic field inside the solenoid is directly proportional to the current flowing through it. This proportionality enables precise control and repeatability in the calibration process. In the experimental setup, a direct current (DC) power supply was used to drive the solenoid, with the current simultaneously monitored via the power supply display to ensure accuracy.

To characterize the generated magnetic field, a Gauss meter (FWBELL-5180) was used to measure the magnetic flux density inside the solenoid, as shown in Figure. 3-3. The measured data was analyzed and fitted to a linear relationship, confirming the expected proportionality between current and magnetic field strength.

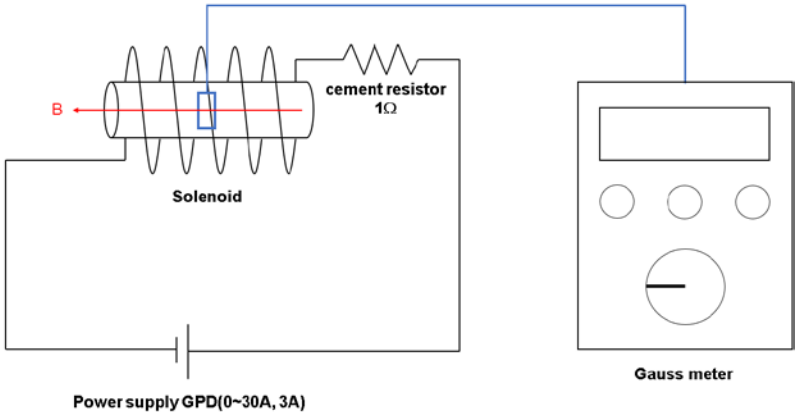

Figure. 3-3 Schematic of the solenoid calibration experiment.

3.3 B-dot probe calibration

To determine the calibration factor C_{calib} of the B-dot probe, a controlled experimental setup was established, as shown in Figure. 3-4. The calibration process involves generating a well-defined pulsed magnetic field inside a solenoid and comparing the induced voltage from the B-dot probe with the inferred magnetic field strength.

A high-voltage power supply (HB-Z103-20AC) was utilized to charge a 993-μF capacitor up to approximately 1 kV. Once fully charged, a spark gap was triggered through self-breakdown, initiating a high-pulsed discharge current of approximately 3 kA through the solenoid. This transient current generates a time-varying magnetic field $B(t)$ inside the solenoid, which is sensed by the B-dot probe positioned within the solenoid's core. The induced voltage from the B-dot probe is recorded using an oscilloscope for further analysis.

In parallel, the discharge current flowing through the solenoid is monitored using a Pearson current monitor (Model 301x), ensuring accurate measurement of the transient current. Since the B-dot probe operates based on Faraday's Law, its output voltage is proportional to the time derivative of the magnetic field. By integrating the induced voltage and comparing it with the known current waveform, the magnetic field can be inferred. The calibration factor C_{calib} is then determined using equation (4).

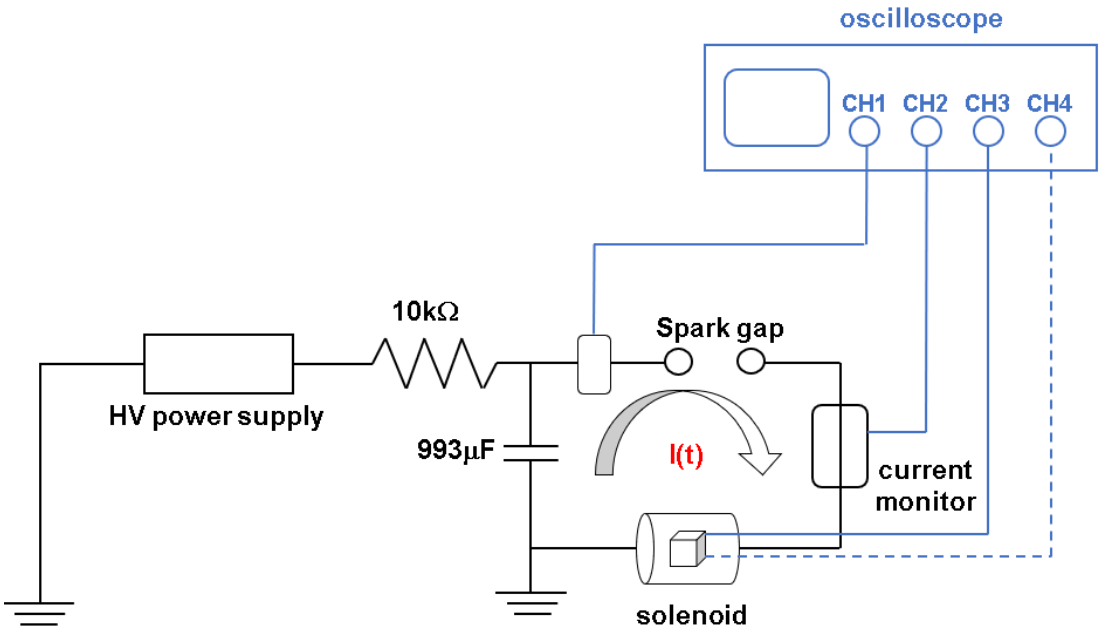

Figure. 3-4 Schematic of the B-dot probe calibration experiment. (CH1: $V_{in}(t)$、CH2: I(t)、CH3: $V_{meas,1}(t)$、CH4: $V_{meas,2}(t)$)

Chapter 4 Result and discussion

This chapter presents the calibration procedures and data processing methods used to validate the performance of the three-axis B-dot probe. The solenoid calibration confirmed a linear relationship between magnetic field and current, providing a reliable reference field. Two coil winding configurations were compared, and the same-direction winding was adopted due to negligible common-mode noise and improved sensitivity. Additionally, the integration-based analysis was replaced with a differentiation approach to eliminate offset-induced errors. Calibration across all three axes demonstrated consistent trends aligned with theoretical expectations, confirming the accuracy and enhanced performance of the redesigned probe system.

4.1 Solenoid calibration

The magnetic field generated inside the solenoid was experimentally measured, as shown in Figure. 4-1. The results demonstrated a clear linear relationship between the magnetic field B and the input current $I(t)$, allowing the data to be fitted using a linear regression model. The slope k of each fitted line, which represents the sensitivity of the magnetic field to the applied current (in units of G/A), varied slightly across five repeated measurements. The average slope was calculated to be 3.272 with a standard deviation of 0.117.

To enhance the accuracy and consistency of the analysis, the intercept of the linear fit was deliberately set to zero. This approach is grounded in the theoretical model, which posits a direct proportionality between the magnetic field and the current. According to this model, when the current is zero, the magnetic field should also be zero. By anchoring the intercept at zero, the physical significance of the model is better preserved, minimizing measurement errors and mitigating the influence of zero-point drift. Consequently, this adjustment enhances the consistency and reliability of the

experimental data.

The resulting linear regression equation representing the magnetic field is given by:

$$B = (3.3 \pm 0.1) \times I(t) \ \ [\mathrm{G}] \approx 3.3 \times 10^{-4} \times I(t) \ [\mathrm{T}] \, . \qquad (7)$$

The observed variation in the slope is likely due to minor inconsistencies in probe positioning and measurement fluctuations. Despite these variations, the linear relationship between the magnetic field and current remains consistent, supporting the theoretical model.

Notably, the experimental results show a slight deviation from the theoretical prediction provided by Equation (5). This discrepancy is likely due to non-uniformities introduced by the drilled hole for probe insertion and possible edge effects at the solenoid ends. The minor offsets observed in the measurements further suggest that the magnetic field inside the solenoid may not be perfectly uniform, potentially due to the geometric imperfections in the solenoid construction.

To minimize these sources of error, future measurements could benefit from improved probe alignment and enhanced solenoid design. The consistency of the linear trend, however, validates the use of the solenoid as a reliable reference field for calibrating the B-dot probe.

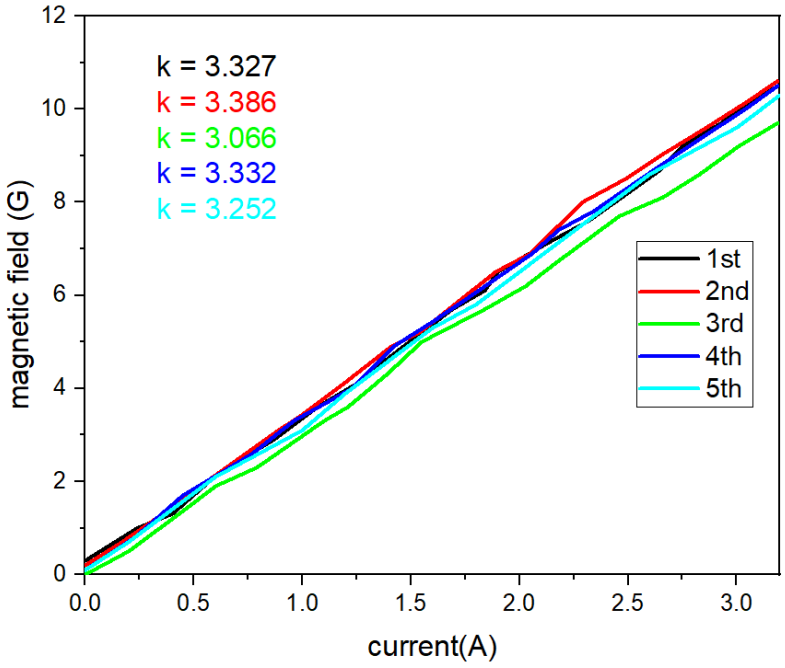

Figure. 4-1 Linear relationship between magnetic field and current inside the solenoid. (k : the sensitivity of the magnetic field response to the input current (G/A))

4.2 Three-axis B-dot probe calibration

4.2.1 Common noise cancelled

In traditional B-dot probe designs, winding the coils in opposite directions along the same axis is commonly employed to cancel capacitive or electrostatic pickup. This configuration effectively eliminates the capacitive coupling by generating equal but opposite electrostatic signals, which cancel each other out. As illustrated in Figure. 3-2, the measured voltage is calculated as follows:

$$V_{\text{meas}} = (V_{\text{meas},2} - V_{\text{meas},1})/2 = [V_{\text{B}} + V_{\text{E}} - (-V_{\text{B}} + V_{\text{E}})]/2 = V_{\text{B}} \ . \quad (9)$$

where V_{B} is the voltage induced by the changing magnetic flux, V_{E} is the capacitive or electrostatic signal.

This method ensures that the output voltage V_{meas} accurately represents the magnetic flux-induced voltage while minimizing capacitive interference. However,

during the experimental measurements, it was observed that the curves of V_{meas} and $V_{\text{meas,2}}$ showed close overlap, indicating minimal common noise, as shown in Figure. 4-2. This observation suggests that the common mode noise between the two signals is negligibly small, which implies that the capacitive or electrostatic interference is inherently low in the current setup.

Based on this finding, it was determined that winding the coils in the same direction along the same axis would be a more practical approach. This configuration simplifies the manufacturing process and allows for more turns to be wound on the coil, thus enhancing the sensitivity of the B-dot probe. Additionally, since the common noise is already minimal, the need for opposing windings to cancel out capacitive pickup is not necessary in this case.

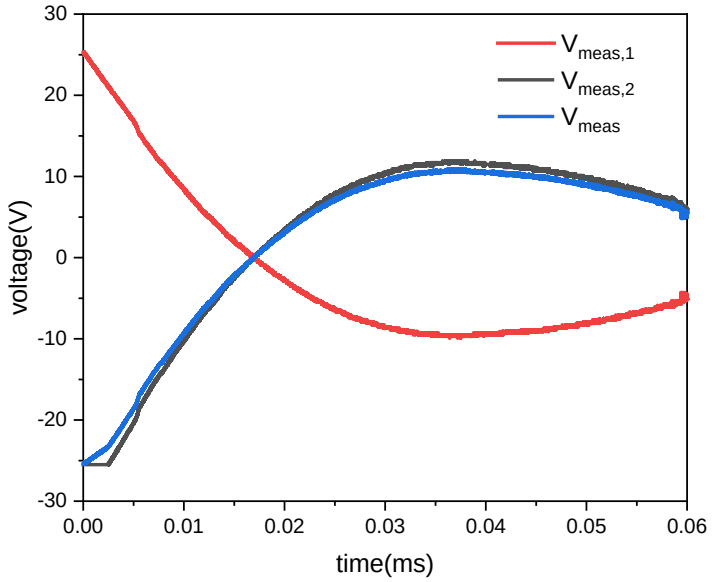

Figure. 4-2 Comparison of V_{meas} and $V_{\text{meas,2}}$

4.2.2 Comparison of integrated & differential method for data analysis

To improve the accuracy and reliability of the three-axis B-dot probe system, this study implemented two key modifications: a new data processing method using differentiation instead of integration, and a revised coil winding configuration with coils wound in the same direction along the same axis. The differentiation method effectively reduces the influence of constant offsets, while the new coil winding design simplifies the manufacturing process and enhances measurement sensitivity. With these improvements, the probes were constructed and tested to evaluate their performance under the modified configuration.

During the calibration of the three-axis B-dot probe, it was observed that the processed data did not exhibit a linear distribution as theoretically expected. Specifically, the voltage signals obtained from the integration of the induced electromotive force deviated from the anticipated linear relationship, as illustrated in Figure. 4-3. This discrepancy suggests the presence of underlying factors influencing the measurement accuracy.

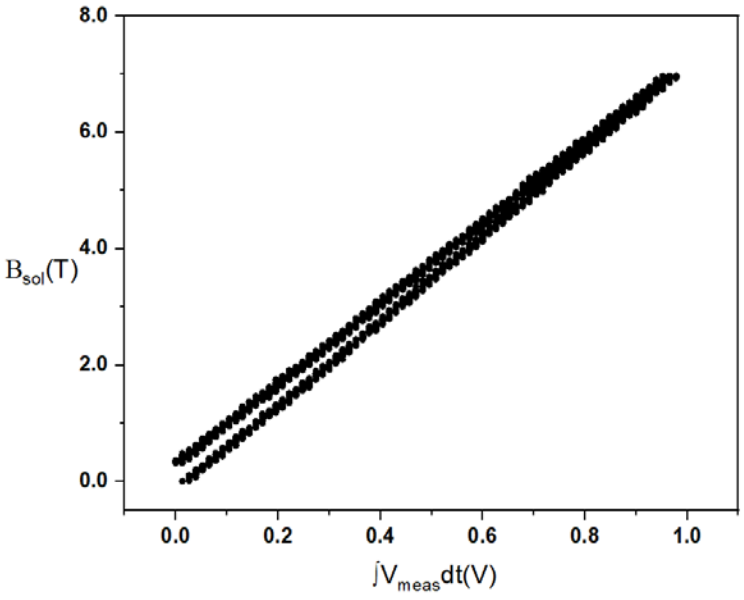

Figure. 4-3 Data processing result using integration method.

One potential cause of this deviation is the effect of constants introduced during the integration process. When integrating the induced voltage to obtain the magnetic flux, any constant offset present in the raw data propagates through the integration, leading to cumulative errors that distort the linearity of the resultant signal. This effect becomes particularly pronounced when dealing with high-frequency noise or baseline drift, which can introduce non-physical trends in the integrated data.

To address this issue, the data processing method was modified by replacing integration with differentiation. This adjustment was derived from Equation (4), where the magnetic field $B(t)$ is calculated by integrating the measured voltage $V_{\text{meas}}(t)$. The modification can be explained more clearly using the following equation:

$$B(t) = -C_{\text{calib}} \int V_{\text{meas}}(t)dt + \varphi \rightarrow \frac{dB(t)}{dt} = -C_{\text{calib}} V_{\text{meas}}(\text{t}) \,. \qquad (8)$$

As a result of this adjustment, the processed data displayed a significantly improved linear distribution, as shown in Figure. 4-4, validating the effectiveness of the differentiation method. This enhancement not only improves the accuracy of the B-dot probe measurements but also ensures a more reliable calibration procedure, thereby enhancing the overall performance of the three-axis magnetic field sensing system.

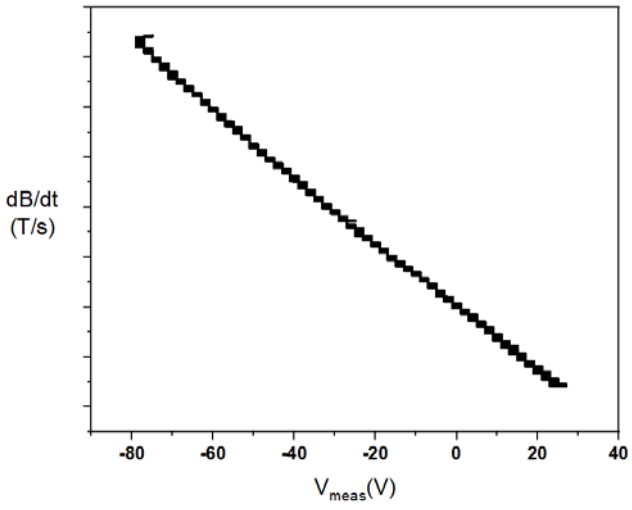

Figure. 4-4 Linear relationship between dB/dT and V_{meas}.

4.2.3 Calibration in 3 axis

Experiments were conducted on each axis using the experimental setup illustrated in Figure. 3-3, which was designed to independently measure the B_x, B_y, B_z components of the magnetic field. From Figure. 3.1(a), it can be observed that the cross-sectional area sizes of each axis follow the order of $B_z > B_x > B_y$. This order corresponds to the physical design of the probe, where the cross-sectional area affects the magnitude of the induced voltage. Due to the differences in cross-sectional area, the calibration magnitudes for each axis vary accordingly. Averaging the data shows that the calibration magnitude follows the trend: B_y $(-136.77 \pm 1.01) > B_x$ $(-128.87 \pm 0.53) > B_z$ (-128.87 ± 0.53). The experimental results align with the theoretical model $C_{\text{calib}} = -\frac{1}{NA} = -312.5$, which predicts an inverse relationship between the calibration constant and the number of turns multiplied by the cross-sectional area. In this experiment, the number of turns is kept constant, and the differences in calibration magnitudes are attributed to the variations in cross-sectional areas. The observed trend in the calibration values is consistent with the theoretical expectations, supporting the effectiveness of the newly implemented data processing method and coil winding configuration. These modifications enhance the accuracy and sensitivity of the three-axis B-dot probe system, confirming the improved performance of the newly designed probes.

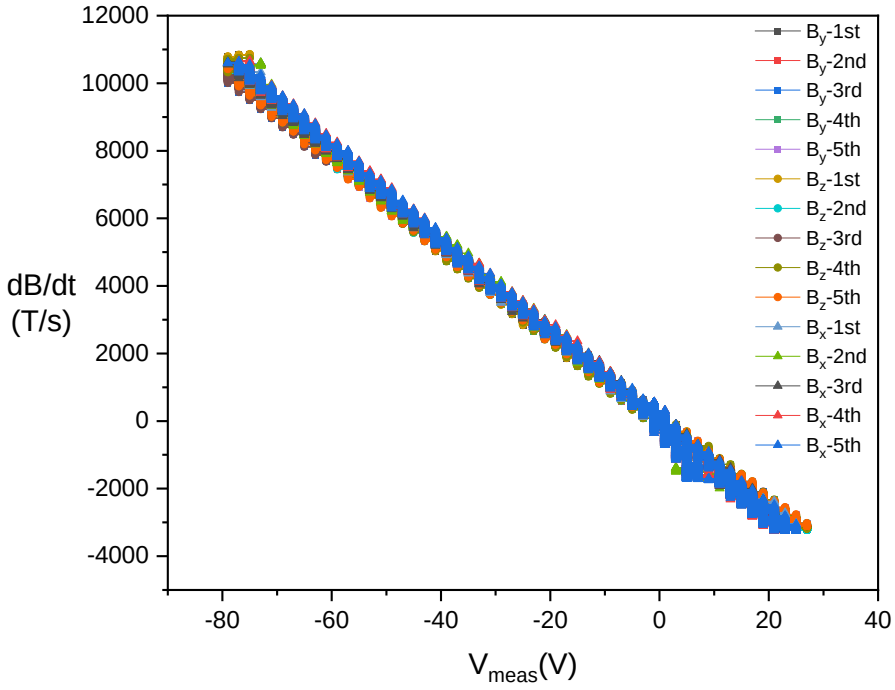

Figure. 4-5 The result of repeated calibration tests for all axes.

Chapter 5 Conclusion

In conclusion, this study successfully demonstrated the stable performance of the three-axis B-dot probe in magnetic field measurements. The probe features three orthogonal loops, each consisting of 32 turns of enameled wire wound on a 10×10×10 mm^3 core.

The probe exhibited low noise interference, as evidenced by the strong overlap between V_{meas} and $V_{meas,2}$, effectively suppressing common noise. Furthermore, the solenoid's calibration value, $B = 3.372\times10^{-4}I(t)$ [T], validated the accuracy of the calibration process. During the calibration process, a solenoid driven by a high-pulse current was utilized to generate a known magnetic field, enabling measurement of the probe's response. To reduce errors associated with numerical integration, the data was processed through differentiation before comparing the probe's output voltage V_{meas} with the rate of change of magnetic flux, $\frac{dB}{dt}$. The calibration constants were determined to be $C_{calib,x} = -128.87 \pm 0.53$, $C_{calib,y} = -136.77 \pm 1.01$, and $C_{calib,z} = -127.75 \pm 6.25$, confirming the inverse relationship between calibration and the loop's cross-sectional area.

In summary, the three-axis B-dot probe is a reliable diagnostic tool for magnetic field measurements, providing stable data support. Future work will focus on the development of a 3-axis Helmholtz coil system for generating uniform magnetic fields and modular B-dot probe arrays for flexible and high-accuracy field assessments.

Chapter 6 Future work

In future work, several potential improvements can be considered to enhance the performance and reliability of the experimental setup. One suggestion is to redesign the probe as an independent component, reducing its direct connection to signal transmission wires. This could prevent damage to both the probe and the wires caused by accidental pulling or external forces during experiments, increasing the system's durability and operational reliability.

Another possible improvement is to implement a hardware-based integrator. Unlike software integration, which may introduce errors, a physical integrator could provide more accurate results, significantly improving the precision of experimental data.

Additionally, the use of Helmholtz coils to generate uniform magnetic fields in three dimensions for probe calibration could be highly beneficial. By arranging Helmholtz coils along the X, Y, and Z axes, a three-dimensional magnetic field can be created, allowing the probe to accurately detect and respond to magnetic field variations in all directions, leading to more precise calibration.

Finally, the development of a removable three-dimensional magnetic probe system (RTMP) could offer flexibility in measuring magnetic fields in three-dimensional space. This system would be useful for evaluating the magnetic null point and assessing the impact of stray magnetic fields on plasma breakdown. The RTMP system, composed of multiple magnetic probes capable of capturing detailed magnetic field variations, would allow for easy repositioning or recalibration, depending on experimental needs, thereby enhancing the adaptability and precision of the experimental setup.

Appendix

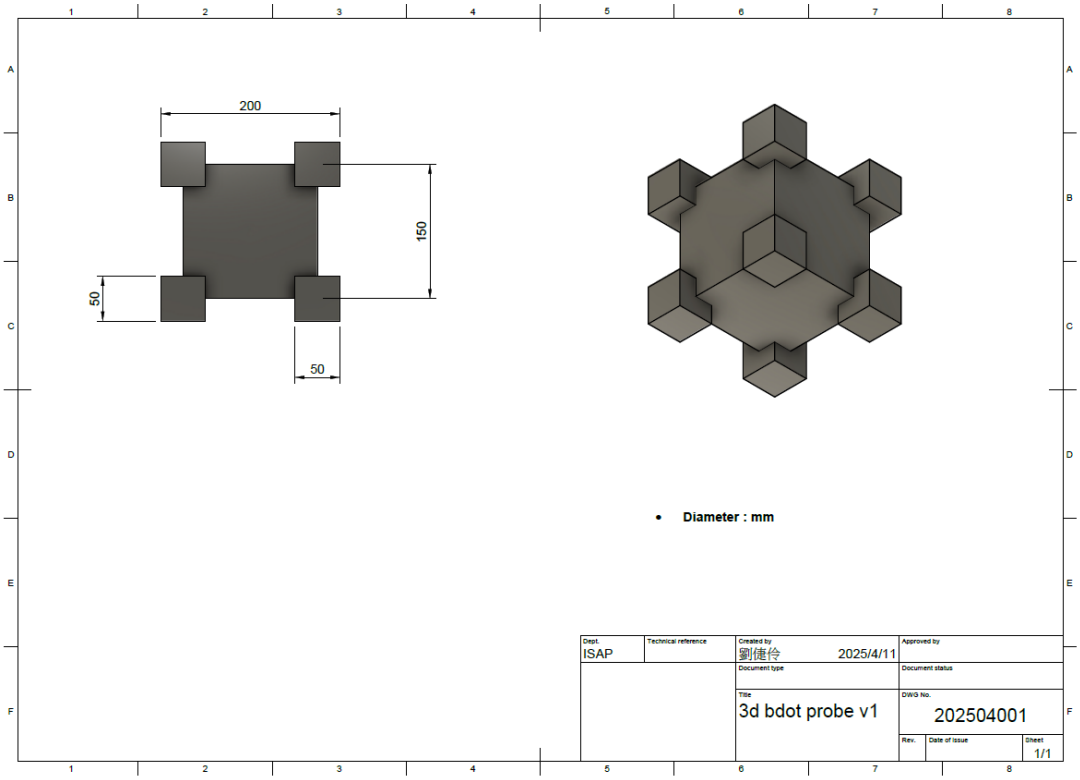

Figure. 1 Engineering drawing of three-axis B-dot probe

Table. 1 References for figures

	Reference	Folder (raw data)
Figure. 4-1	solenoid calibration.opju	/Experiments/2024_jliu2/solenoid calibration
Figure. 4-2	ANALYSIS.opju	/Experiments/2024_jliu2/20240808
Figure. 4-3	ANALYSIS.opju	/Experiments/2024_jliu2/20240812
Figure. 4-4	ANALYSIS.opju	/Experiments/2024_jliu2/20240812
Figure. 4-5	ANALYSIS.opju	/Experiments/2024_jliu2/20240830